CD47 Blockade Leads to Chemokine-Dependent Monocyte Infiltration and Loss of B Cells from the Splenic Marginal Zone

Ying Ying Yiu,*,† Paige S. Hansen,*,‡ Laughing Bear Torrez Dulgeroff,* Grace Blacker,* Lara Myers,§ Sarah Galloway,* Eric Gars,¶ Olivia Colace,* Paul Mansfield,* Kim J. Hasenkrug,§ Irving L. Weissman,*,¶,‖,# and Michal Caspi Tal*,‡

CD47 is an important innate immune checkpoint through its interaction with its inhibitory receptor on macrophages, signal-regulatory protein α (SIRPα). Therapeutic blockade of CD47–SIRPα interactions is a promising immuno-oncology treatment that promotes clearance of cancer cells. However, CD47–SIRPα interactions also maintain homeostatic lymphocyte levels. In this study, we report that the mouse splenic marginal zone B cell population is dependent on intact CD47–SIRPα interactions and blockade of CD47 leads to the loss of these cells. This depletion is accompanied by elevated levels of monocyte-recruiting chemokines CCL2 and CCL7 and infiltration of $CCR2^{+}Ly6C^{hi}$ monocytes into the mouse spleen. In the absence of CCR2 signaling, there is no infiltration and reduced marginal zone B cell depletion. These data suggest that CD47 blockade leads to clearance of splenic marginal zone B cells. ***The Journal of Immunology*****, 2022, 208: 1371–1377.**

CD47 is a transmembrane glycoprotein found on the cell surface and serves as a "marker of self" (1, 2). CD47 binding to signal-regulatory protein α (SIRPα) acts as an important signaling axis in immune cell clearance and inflammatory signaling. Upon CD47 engagement of SIRPα receptors on phagocytes, phosphorylation of cytoplasmic ITIM motifs by protein tyrosine phosphatases SHP-1 and/or SHP-2 inhibits the cytoskeletal changes required for macrophage phagocytosis (3). As opposed to mechanisms that facilitate the clearance of dead cells, phagocytic clearance of live cells through programmed cell removal (PrCR) is largely controlled by CD47–SIRPα interactions (4–6). For example, high expression of CD47 in young RBCs protects them from cell clearance through interaction with SIRPα on macrophages (1). As erythrocytes age, they lose this important anti-phagocytic signal, leading to their clearance by splenic macrophages (1, 7). Accordingly, transient anemia has previously been reported following CD47 blockade in vivo (8). Circulating hematopoietic stem cells also highly upregulate CD47, presumably to avoid phagocytic clearance, and efficient transplantation of multiple hematopoietic cell types has been shown to be dependent on CD47 expression (9–11).

Malignant cells, including leukemias, lymphomas, and solid tumors, upregulate cell surface CD47 to evade phagocytic clearance (8, 9, 12). The physiological relevance of CD47 upregulation is illustrated by the fact that blocking CD47 with Abs in vitro causes the increased phagocytosis of various cancer cell types by macrophages. More importantly, in mouse models of human malignancies, anti-CD47 mAbs promote PrCR of leukemias (9, 13, 14) and synergize with anti-tumor mAbs such as rituximab, trastuzumab, cetuximab, and panitumumab to enhance the elimination of aggressive cancers (13, 15–18). CD47 blockade has emerged as a promising therapeutic strategy in modulating the immune system to reduce or prevent metastases (8, 19) and is currently being tested in multiple clinical trials. Therefore, further investigation of the effects that CD47 blockade has on the immune system is necessary.

CD47–SIRPα interactions have been shown to affect homeostatic lymphocyte frequencies, activation status, and Ab production in a humanized mouse model (10). Additionally, non-malignant murine B cells from $CD47^{-/-}$ mice are more prone to Ab-dependent phagocytosis when targeted with anti-CD19 mAb (20). Disruption of the negative signaling protein SHIP has been shown to result in the loss

*Institute for Stem Cell Biology and Regenerative Medicine and the Ludwig Cancer Center, Stanford University School of Medicine, Stanford, CA; †Immunology Program, Stanford University, Stanford, CA; ‡Department of Biological Engineering, Massachusetts Institute of Technology, Cambridge, MA; §Laboratory of Persistent Viral Diseases, Rocky Mountain Laboratories, National Institute of Allergy and Infectious Diseases, National Institutes of Health, Hamilton, MT; ¶Department of Pathology, Stanford University School of Medicine, Stanford, CA; ‖Ludwig Center for Cancer Stem Cell Research and Medicine, Stanford University School of Medicine, Stanford, CA; and #Stanford Cancer Institute, Stanford University School of Medicine, Stanford, CA

ORCIDs: 0000-0002-9800-8099 (Y.Y.Y.); 0000-0002-2040-4788 (G.B.); 0000-0003-0221-9770 (L.M.); 0000-0003-0850-402X (S.G.); 0000-0001-8523-4911 (K.J.H.); 0000-0003-2550-6246 (M.C.T.).

Received for publication April 13, 2021. Accepted for publication January 11, 2022.

This work was supported by funds from the Virginia and D.K. Ludwig Fund for Cancer Research, the Robert J. Kleberg, Jr. and Helen C. Kleberg Foundation, and the Intramural Research Program of the National Institute of Allergy and Infectious Diseases, National Institutes of Health. M.C.T. and Y.Y.Y. were supported by a Stanford Immunology Training Grant (National Institutes of Health Grant 5T32AI007290). M.C.T. was also supported by National Institutes of Health NRSA Grant 1 F32 AI124558-01, the Fairbairn Family Foundation, and by the Bay Area Lyme Foundation. Y.Y.Y. was also supported by National Science Foundation GRFP Grant DGE-1147470. L.B.T.D. was supported by the Stanford Diversifying Academia, Recruiting Excellence fellowship.

Y.Y.Y. and M.C.T. conceived and performed experiments, analyzed and interpreted data, and wrote the manuscript. P.S.H. performed experiments, analyzed data, contributed ideas, and wrote the manuscript. G.B. performed experiments, analyzed data, and contributed ideas. L.B.T.D. and L.M. performed experiments, contributed ideas, and wrote the manuscript. S.G. and P.M. performed experiments. O.C. edited the manuscript. E.G. analyzed data. K.J.H. interpreted results and edited the manuscript. I.L.W. conceived experiments, interpreted results, and edited the manuscript. K.J.H., I.L.W., and M.C.T. supervised the research.

Irving L. Weissman is a Distinguished Fellow of AAI.

Address correspondence and reprint requests to Prof. Irving L. Weissman and Dr. Michal Caspi Tal, Stanford University School of Medicine, Stanford, CA. E-mail addresses: irv@stanford.edu (I.L.W.) and mtal@mit.edu (M.C.T.)

The online version of this article contains supplemental material.

Abbreviations used in this article: FOL, follicular; m, murine; KO, knockout; MZ, marginal zone; PrCR, programmed cell removal; PS, phosphatidylserine; RT, room temperature; SIRPα, signal-regulatory protein α; WT, wild-type.

of marginal zone (MZ) B cells and reorganization of MZ macrophages (MZMs) to the red pulp of the spleen (21). Given that SHIP is involved in CD47–SIRPα interactions, we investigated how CD47 blockade affects healthy B cells and, specifically, MZ B cells in vivo.

Materials and Methods

Mice and in vivo CD47 blockade

Wild-type (WT) C57BL/6J mice (no. 000664) and B6.129(Cg)-*Ccr2*$^{tm2.1Ifc}$/J (CCR2 knockout [KO]) mice (no. 017586) were purchased from The Jackson Laboratory. CCR2KO mice were subsequently bred in-house. Eight- to 16-wk-old female mice were used for all experiments. For in vivo experiments, mice were given 100 µl of PBS (Life Technologies), mouse IgG1 isotype control (Bio X Cell), or anti-CD47 mAb clone MIAP410 (anti-CD47 mAb) (Bio X Cell) by i.p. injection. On day 0, 100 µg in 100 µl is given to each mouse. During the course of 2 wk, on days 3, 5, 7, 10, 12, and 14, each mouse received 500 µg in 100µl. Spleens were harvested on day 17 or day 24. Peripheral blood was collected into EDTA tubes via cardiac puncture and centrifuged. Plasma was transferred and frozen at −80°C. Because immune cell populations were similar in mice treated with PBS and mIgG1 isotype control, PBS was used in some experiments as a control for anti-CD47 mAb treatment involving WT mice to minimize costs.

In vitro CD47 blockade

Single-cell suspensions were prepared from spleens of female WT C57BL/6J mice as described above. An EasySep mouse B cell isolation kit was purchased from STEMCELL Technologies (no. 19854) and B cells were enriched from splenocytes following the manufacturer's protocol. Briefly, splenocytes were resuspended in PBS containing 2% FBS and 1 mM EDTA at 1×10^8 cells/ml. Rat serum was added, followed by an isolation cocktail, and samples were incubated at room temperature (RT) for 10 min. RapidSpheres magnetic beads were then added and samples were incubated for 2.5 min at RT. The samples were placed in the magnet for 2.5 min at RT and the non-magnetic portion was collected and washed with RPMI 1640 (Life Technologies) supplemented with 10% FBS and 100 U/ml penicillin and 100 µg/ml streptomycin (R10; Life Technologies). Enriched B cells or splenocytes were seeded at a density of 1×10^6 splenocytes per well of a 96-well U-bottom tissue culture plate. Cells were then treated with PBS, 10 µg/ml LPS, mIgG1 isotype control, and/or anti-CD47 mAb MIAP410. Cells were collected at 24 h poststimulation for analysis by flow cytometry.

Flow cytometry

Spleens were collected into PBS (Life Technologies) and moved to R10 for dissociation. Spleens were dissociated mechanically with a razor, digested with 10% collagenase IV (Sigma-Aldrich) and 1% DNase I (Sigma-Aldrich) in R10 for 30 min at 37°C, washed with media, and passed through 70-µm strainers. The single-cell suspension was then lysed with ACK (ammonium-chloride-potassium) lysis buffer (Life Technologies), resuspended into PBS with 2% FBS (FACS buffer), stained with Abs, and immediately analyzed on an LSRFortessa. The following Abs were used: PerCP-Cy5.5 anti-B220 (clone RA3-6B2, BioLegend), FITC anti-mCD21/35 (clone 7E9, BioLegend), PE anti-mCCR2 (clone SA203G11, BioLegend), PE-Cy7 anti-mCD93 (clone AA4.1, BioLegend), allophycocyanin anti–murine (m)IgM (clone RMM-1, BioLegend), AF700 anti-mCD19 (clone 6D5, BioLegend), allophycocyanin-Cy7 anti-mCD23 (clone B3B4, BioLegend), BV605 anti-mIgM (clone RMM-1, BioLegend), allophycocyanin anti-mIgD (clone 11-26c.2a, BioLegend), allophycocyanin-Cy7 anti-mIgM (clone RMM-1, BioLegend), FITC anti–m/human CD11b (clone M1/70, BioLegend), PE-Cy7 anti-mLy6C (clone HK1.4, BioLegend), AF700 anti-mLy6G/Ly6C (Gr-1) (clone RB6-8C5, BioLegend), PE anti-calreticulin (clone FMC 75, Enzo Life Sciences), and PE anti-mCD47 (clone MIAP301, BioLegend). PE-annexin V and annexin V binding buffer were purchased from BioLegend. Data were collected on a FACS LSRFortessa or FACSymphony (BD Biosciences) and analyzed with FlowJo software.

Immunofluorescence

Fresh spleen tissues were embedded and frozen in Tissue-Tek OCT compound (VWR) and cut into 5-µm sections. Slides were fixed in −20°C acetone for 10 min, blocked with 10% rat serum in PBS, and stained for 1 h at RT with the following primary mAbs: rat anti-mouse CD1d (clone 1B1, Bio-Rad), AF647-conjugated rat anti-mouse CD1d (clone 1B1, BD Biosciences), rabbit anti-mouse MARCO (R&D Systems), and FITC-conjugated rat anti-mouse MOMA-1 (Thermo Fisher Scientific). Unconjugated Abs were further

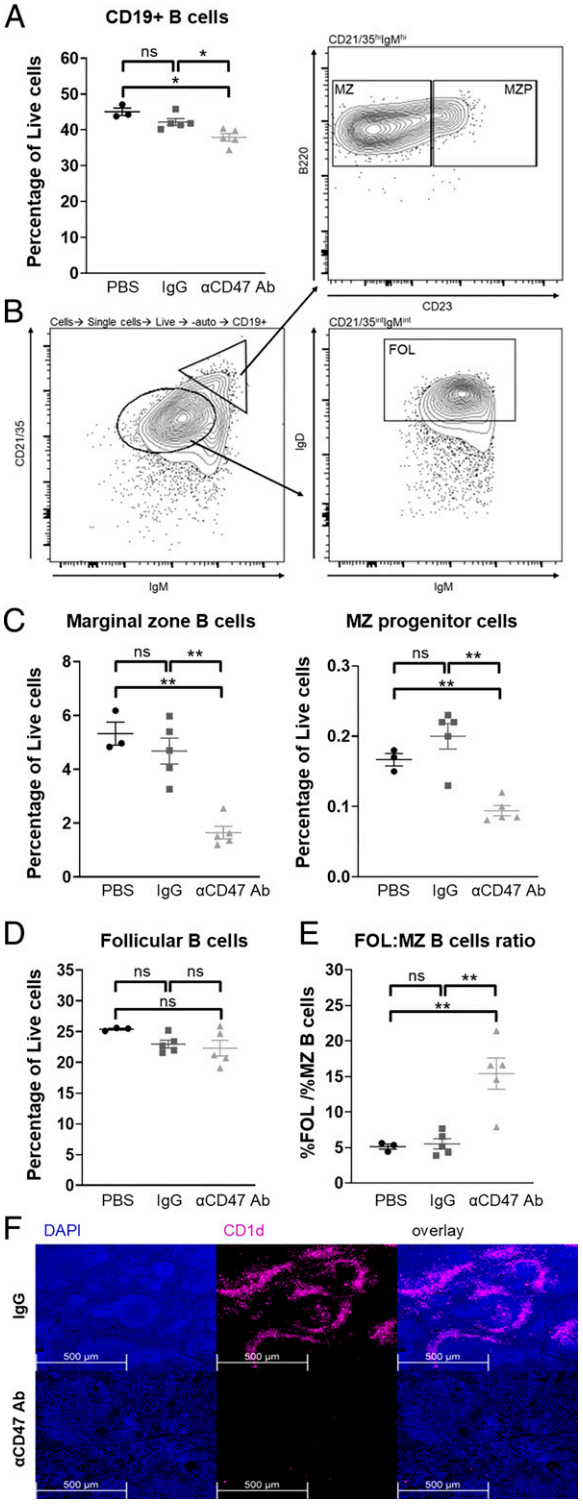

FIGURE 1. Anti-CD47 mAb treatment depletes splenic MZ B cells. WT C57BL/6 mice were injected with PBS, IgG isotype control, or anti-CD47 Ab i.p. as described in *Materials and Methods*. (**A**) Percentage of CD19$^+$ splenic B cells. (**B**) FACS plots illustrating the gating strategy for MZ, MZ progenitor (MZP), and follicular (FOL) B cells. (**C**–**E**) Percentage of (C) MZ and MZP B cells and (D) FOL B cells in mice treated with PBS, IgG isotype control, or anti-CD47 Ab and (E) the ratio of FOL/MZ B cells in these mice. All data are representative of at least three independent experiments with three to five mice per group. Groups were compared with an unpaired, two-tailed *t* test with Welch's correction. Data are presented as the mean ± SEM. (**F**) Representative images of immunofluorescence staining of MZ B cells in spleens of mice treated with PBS or anti-CD47 Ab. Sections were stained with AF647-conjugated rat anti-mouse CD1d mAb and DAPI. $*p < 0.05$, $**p < 0.01$; ns, not significant.

detected with AF647 or AF555 goat anti-rabbit and goat anti-rat secondary Abs (Thermo Fisher Scientific). Sections were stained with DAPI (BioLegend), mounted with ProLong diamond antifade mountant (Thermo Fisher Scientific) and imaged with a Leica DM5500B upright microscope.

Immunohistochemistry

Spleen tissues were fixed with 4% paraformaldehyde overnight and stored in 70% ethanol. Histology was performed by HistoWiz using a standard operating procedure and fully automated workflow. Samples were processed, embedded in paraffin, and sectioned at 4 μm. Immunohistochemistry was performed on a BOND RX autostainer (Leica Biosystems) with enzyme treatment (1:1000) using standard protocols. Abs used were rat monoclonal B220 primary Ab (Novus Biologicals, NB100-77420, 1:200) and rabbit anti-rat secondary Ab (Vector Laboratories, 1:100). A BOND polymer refine detection kit (Leica Biosystems) was used according to the manufacturer's protocol. After staining, sections were dehydrated and film was coverslipped using a Tissue-Tek Prisma and Coverslipper (Sakura). Whole-slide scanning (×40) was performed on an Aperio AT2 (Leica Biosystems).

Luminex

Frozen plasma samples were transferred to the Human Immune Monitoring Center at Stanford University, which performed the assay. Mouse 38-plex Procarta kits were purchased from eBioscience/Affymetrix/Thermo Fisher Scientific (Santa Clara, CA) and used according to the manufacturer's recommendations with modifications as described. In brief, beads were added to a 96-well plate and washed in a BioTek ELx405 washer. Samples were added to the plate containing the mixed Ab-linked beads and incubated at RT for 1 h followed by overnight incubation at 4°C with shaking. Cold (4°C) and RT incubation steps were performed on an orbital shaker at 500–600 rpm. Following the overnight incubation plates were washed in a BioTek ELx405 washer and then biotinylated detection Ab was added for 75 min at RT with shaking. The plate was washed as above and streptavidin-PE was added. After incubation for 30 min at RT wash was performed as above and reading buffer was added to the wells. Each sample was measured in duplicate. Plates were read using a Luminex 200 or a FM3D FlexMap instrument with a lower bound of 50 beads per sample per cytokine. Custom AssayCheX control beads were purchased from Radix Biosolutions (Georgetown, TX) and were added to all wells.

Statistical analysis

Statistical analyses were performed using GraphPad Prism software, with specific details of the tests performed indicated in each figure legend.

Results

Anti-CD47 mAb treatment depletes splenic MZ B cells

WT C57BL/6 mice were treated either with PBS, mouse IgG1 isotype control, or anti-CD47 mAb MIAP410 i.p. for 2 wk as described in *Materials and Methods*, and B cell populations in the spleen were analyzed by flow cytometry. CD47 blockade led to depletion of $CD19^+$ cells in the spleen of treated animals compared with PBS or IgG controls (Fig. 1A). Two major subsets of B cells in the spleen are $CD19^+B220^+CD21/35^{hi}IgM^{hi}IgD^-$ MZ B cells and $CD19^+CD21/35^{int}IgM^{int}IgD^{hi}$ follicular (FOL) B cells (Fig. 1B). We found that the percentages of $CD19^+B220^+CD21/35^{hi}IgM^{hi}CD23^{lo/-}$ MZ B cells

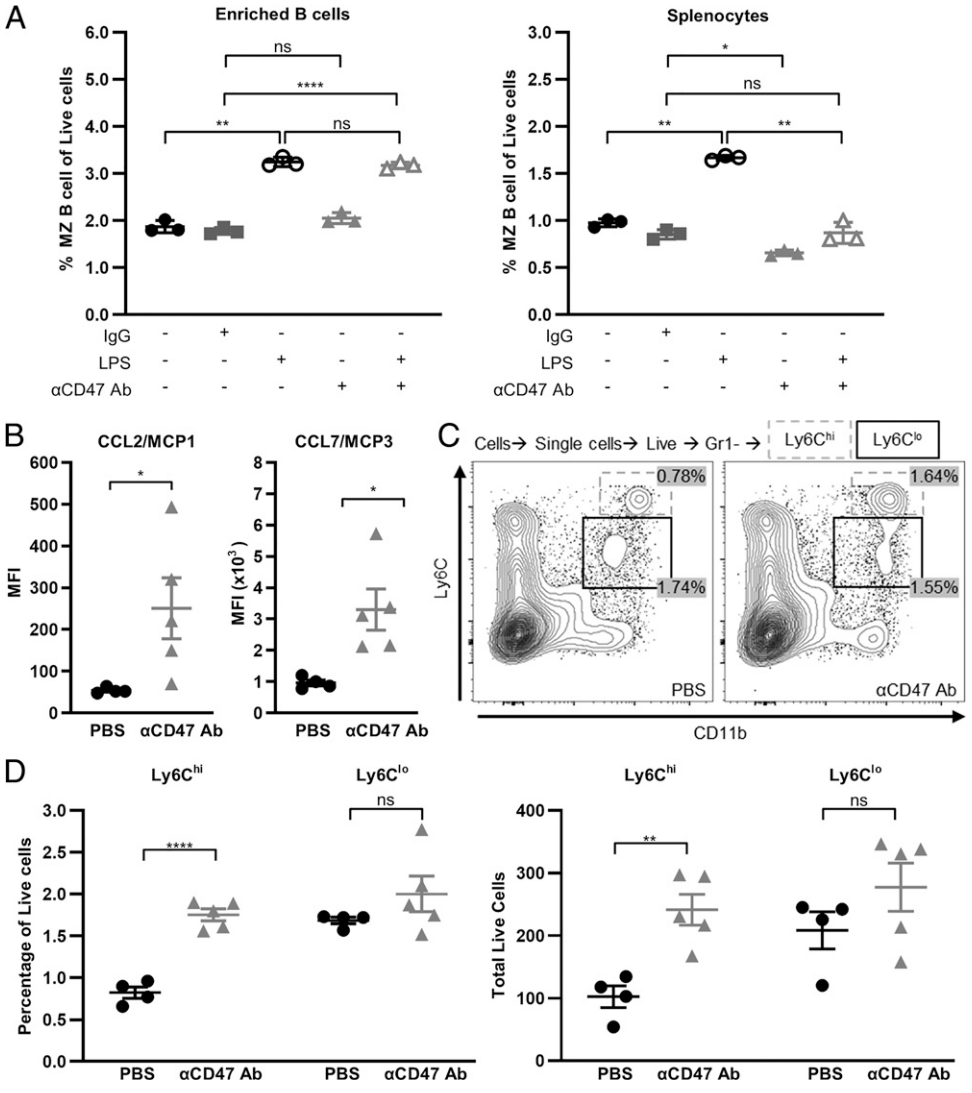

FIGURE 2. MZ B cell depletion is cell extrinsic and associated with monocyte infiltration. (**A**) Magnetically enriched mouse splenic $CD19^+$ cells or mouse splenocytes were cultured and treated with IgG isotype control, LPS, and/or anti-CD47 Ab. Percent of MZ B cells after 24 h of indicated treatment is shown. Groups were compared with a paired, two-tailed *t* test. Data are presented as the mean ± SD. (**B**) Mean fluorescence intensity (MFI) of CCL2 and CCL7 in plasma of mice treated i.p. with PBS or anti-CD47 Ab for 2 wk. (**C**) Representative FACS plots showing percentages of $Ly6C^{hi}$ (dotted box) and $Ly6C^{lo}$ (solid box) monocytes in control versus anti-CD47 mAb–treated mice. (**D**) Percent and absolute number of $Ly6C^{hi}$ and $Ly6C^{lo}$ monocytes in mice treated with PBS or anti-CD47 Ab. Groups were compared with an unpaired, two-tailed *t* test with Welch's correction. Data are presented as the mean ± SEM. $*p < 0.05$, $**p < 0.01$, $****p < 0.0001$; ns, not significant.

and $CD19^+B220^+CD21/35^{hi}IgM^{hi}CD23^+$ MZ progenitor (MZP) cells were both significantly reduced in mice treated with anti-CD47 mAb (Fig. 1C). However, CD47 blockade did not impact $CD19^+CD21/35^{int}IgM^{int}IgD^{hi}$ FOL B cells (Fig. 1D). Comparison of the ratio of FOL to MZ B cells further shows a specific and significant increase in MZ B cells in treated mice compared with PBS and IgG control mice (Fig. 1E). Immunofluorescence staining of the spleens of MIAP410-treated animals confirms the depletion of MZ B cells, as demonstrated by significantly diminished expression of CD1d, a marker for MZ B cells (Fig. 1F). Furthermore, immunohistochemistry staining shows a decrease in $B220^+$ B cells, in particular in the areas of the red pulp and MZ (Supplemental Fig. 1A). Decreased immunohistochemistry staining of CD21, a marker highly expressed by MZ B cells, further confirms that CD47 blockade leads to loss of splenic MZ B cells (Supplemental Fig. 1B). Taken together, these data show that MZ B cells are especially vulnerable to in vivo depletion in the absence of CD47 signaling.

MZ B cell depletion is cell extrinsic and associated with monocyte infiltration

To determine whether MZ B cell depletion in the spleen was cell intrinsic, we cultured magnetically enriched B cells or whole splenocytes in vitro in the presence of control mouse IgG1 or anti-CD47 mAb overnight. LPS, a component of Gram-negative bacteria that is a TLR4 ligand, was used as a positive control. MZ B cells activate and proliferate in a cell-intrinsic manner when stimulated with LPS (22, 23). As expected, the percentage of MZ B cells increased in both the cultures of enriched B cells and whole splenocytes in the presence of LPS (Fig. 2A). However, the depletion of MZ B cells upon anti-CD47 mAb treatment was only observed with whole splenocytes and not enriched B cells, suggesting that other non–B cell splenic populations were necessary for MZ B cell depletion. Notably, this MZ B cell depletion was sufficient to counterbalance LPS stimulation, leaving the percentage of MZ B cells unchanged when splenocytes were treated with both LPS and anti-CD47 mAb (Fig. 2A).

To explore the cell extrinsic factors that might be responsible for the depletion of MZ B cells upon CD47 blockade, plasma levels of cytokines and chemokines from treated mice were analyzed by Luminex. As previously reported, mice receiving anti-CD47 mAb had elevated plasma CCL2 (MCP1) and CCL7 (MCP3) (Fig. 2B) (24). CCL2 and CCL7 are important cytokines in the recruitment of monocytes, which express CCR2. Given that CD47 blockade promotes phagocytosis by monocytes and macrophages, we investigated whether the depletion of B cells was a result of chemotactic changes and trafficking of monocytic populations into the spleen. $Ly6C^{hi}$ monocytes are a population of inflammatory monocytes that highly express CCR2. They are critical for host defense against certain bacterial and parasitic pathogens and are recruited to tissue sites in a CCR2-dependent manner (25). We found a significant increase in both the percentage and the total number of live $Ly6C^{hi}$ cells in the spleens of treated mice compared with control animals. However, the percentage and total number of splenic $Ly6C^{lo}$ cells were unchanged with CD47 blockade (Fig. 2C, 2D). Indeed, we found that almost all $Ly6C^{hi}$ monocytes expressed CCR2 but only ~40% of $Ly6C^{lo}$ monocytes expressed CCR2 in both control and anti-CD47 mAb–treated mice (Supplemental Fig. 2A). CCR2 expression was much higher on $Ly6C^{hi}$ than $Ly6C^{lo}$ monocytes. Upon CD47 blockade, CCR2 expression remained high on $Ly6C^{hi}$ monocytes and increased on $Ly6C^{lo}$ monocytes (Supplemental Fig. 2B). The higher CCR2 expression by $Ly6C^{hi}$ monocytes likely contributed to their increased infiltration into the spleen in the presence of elevated levels of CCL2 and CCL7. Marginal metallophilic macrophages (MMMs) and MZ macrophages (MZMs) are cell populations that interact closely with MZ B cells. Immunofluorescence staining of MOMA-1 and MARCO, markers for MMMs and MZMs, respectively, showed that anti-CD47 mAb treatment did not significantly alter these populations (data not shown and Supplemental Fig. 3). These data demonstrate that CD47 blockade induces concurrent splenic monocyte infiltration and cell-extrinsic MZ B cell depletion.

MZ B cell depletion is partially rescued and infiltration of $Ly6C^{hi}$ monocytes into the spleen is impaired in CCR2KO mice

To determine whether CCL2/CCL7-CCR2 chemokine signaling is necessary for $Ly6C^{hi}$ monocyte infiltration and MZ B cell depletion upon CD47 blockade, we treated WT and CCR2KO mice with anti-CD47 mAb. CD47 blockade in CCR2KO mice induced a slight but nonsignificant drop in the percentages of $CD19^+$ and MZ B cells, suggesting partial rescue of $CD19^+$ cells and MZ B cells in the absence of CCR2 signaling (Fig. 3A). We did not find significant expression of CCR2 on MZ B cells in control or anti-CD47 mAb–-treated mice (data not shown), so rescue of MZ B cells in CCR2KO mice likely resulted from impacts on the $CCR2^+Ly6C^{hi}$ inflammatory monocytes. Indeed, the percentage of $Ly6C^{hi}$ monocytes in CCR2KO mice treated with anti-CD47 mAb remained unchanged whereas there was a significant increase in their numbers in corresponding WT control mice (Fig. 3C, 3D). Taken together, these results showed that CCR2-dependent recruitment of $Ly6C^{hi}$ monocytes into the spleen correlates with the clearance of MZ B cells.

MZ B cell depletion and recovery are rapid

Cell clearance occurs in minutes whereas MZ B cell turnover occurs over a matter of weeks (26). Therefore, we assessed the extent of MZ B cell depletion within 24 h of administering a single, non-saturating dose of anti-CD47 mAb. We saw a rapid decrease in the percentage of splenic MZ B cells but not that of $CD19^+$ cells or MZP cells (Fig. 4A–C). As cell death could also lead to rapid clearance, we assessed cell permeability of MZ B cells following CD47 blockade with DAPI, a DNA stain. We did not find any decrease in MZ B cell viability with treatment (Supplemental Fig. 4E). As expected, the percentage of FOL B cells was unchanged (Fig. 4D). In

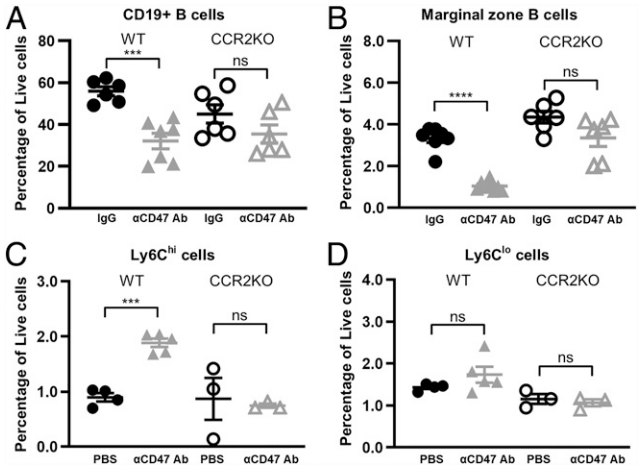

FIGURE 3. MZ B cell depletion is partially rescued and infiltration of $Ly6C^{hi}$ monocytes into the spleen is impaired in CCR2KO mice. (**A**–**D**) Percentage of (A) $CD19^+$ splenic B cells, (B) MZ B cells, (C) $Ly6C^{hi}$, and (D) $Ly6C^{lo}$ in C57BL/6 WT or CCR2KO mice treated with PBS or IgG isotype control or anti-CD47 Ab, as described in *Materials and Methods*. Data are representative of two independent experiments with three to four mice per group (A and B) and one experiment with three to five mice per group (C and D). Groups were compared with an unpaired, two-tailed *t* test with Welch's correction. Data are presented as the mean ± SEM. $***p < 0.001$, $****p < 0.0001$; ns, not significant.

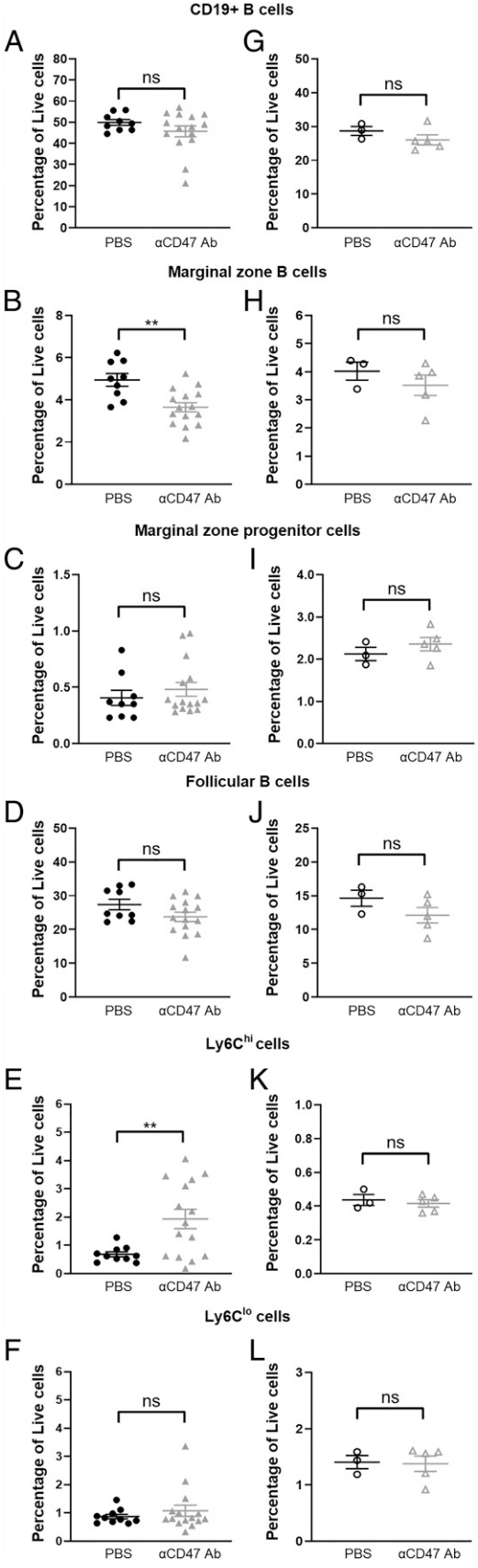

FIGURE 4. MZ B cell depletion and recovery are rapid. (**A–F**) Percentage of (A) $CD19^+$ splenic B cells, (B) MZ and (C) MZP B cells, (D) FOL B cells, and (E) $Ly6C^{hi}$ and (F) $Ly6C^{lo}$ monocytes in C57BL/6 mice 24 h after treatment with PBS or a single, 100-μg dose of anti-CD47 Ab. Data are from two independent experiments with 5–10 mice per group. (**G–L**) Percentage of (G) $CD19^+$ splenic B cells, (H) MZ and (I) MZP B cells, (J) FOL B cells, and (K) $Ly6C^{hi}$ and (L) $Ly6C^{lo}$ monocytes in C57BL/6 mice 24 h after treatment with PBS or anti-CD47 Ab. Spleens were harvested on day 24. Data are from one experiment with three to five mice per group. Groups were compared with an unpaired, two-tailed *t* test with Welch's correction. Data are presented as the mean ± SEM. $^{**}p < 0.01$; ns, not significant.

addition, the percentage of $Ly6C^{hi}$, but not $Ly6C^{lo}$, monocytes increased quickly after treatment (Fig. 4E, 4F). We also found that MZ B cell numbers recovered quickly after discontinuation of CD47 blockade. Within 10 d after the final dose of a 2-wk regimen of anti-CD47 mAb treatment, mice that had previously received a 2-wk course of anti-CD47 mAb had comparable levels of $CD19^+$, MZ, and MZP B cells as mice that received PBS (Fig. 4G–I). FOL B cell numbers remained the same, as expected (Fig. 4J). Accordingly, the infiltration of $Ly6C^{hi}$ monocytes was also resolved, further supporting the correlation between monocyte infiltration and MZ B cell depletion (Fig. 4K, 4L). Given how quickly depletion and recovery of MZ B cells occur, it is likely that CD47 blockade actively promotes ongoing clearance of these cells.

Discussion

We found that B cell frequencies, particularly those of MZ B cells, were decreased in the spleen upon CD47 blockade. MZ B cells are anatomically most exposed to the splenic macrophages that rely on the SIRPα-CD47–mediated "don't eat me" signal to prevent phagocytosis (6). Intriguingly, it has been shown in SIRPα mutant mice that SIRPα signaling plays an important role in maintaining the numbers and localization of MZ B cells (27). Furthermore, mice lacking a key regulator of phagocytosis, SHIP, within their macrophages also had a severe reduction in MZ B cells similar to CD47 blockade (21). SHIP-deficient animals, as well as SHP-1– and SIRPα-deficient animals, have been shown to have enhanced myeloid cell production and reduced IgM^+ B cells, all of which are recapitulated by CD47 blockade (28–32). In contrast to loss of CD47–SIRPα interactions or critical phosphatases that mediate downstream inhibition of ITIM-containing receptors such as SHIP-1 and SHP-1, loss of a critical kinase for PrCR, Bruton's tyrosine kinase (Btk) (33, 34), produced an expanded MZ B cell population (35). Furthermore, KO of BTK from SHIP KO mice rescued the SHIP single KO phenotype of enlarged spleens and loss of MZ B cells (21). Another critical kinase for phagocytosis is MER tyrosine kinase, and knock down of MER tyrosine kinase also led to an enlarged MZ B cell compartment (36). Taken together, these results indicate that macrophage-mediated phagocytic clearance controls both the population size and location of MZ B cells.

The current results indicate that levels of CD47 expression on healthy MZ B cells regulate their population size. MZ B cells have been shown to express moderate levels of CD47 as well as a classic "eat me" signal, phosphatidylserine (PS), normally expressed on apoptotic cells (20, 37). Indeed, we found that MZ B cells express much higher levels of CD47 and PS than do FOL B cells, and CD47 blockade led to increased cell surface PS expression on live MZ B cells (Supplemental Fig. 4A, 4B) but not increased cell death (Supplemental Fig. 4C–F). Importantly, we did not find MZ B cells in the blood or other areas of the spleen by FACS or histology (data not shown), demonstrating that CD47 blockade clears but does not alter localization of MZ B cells. Given the concurrent infiltration of monocytes, blockade of the CD47 don't eat me signal would allow the positive eat me signal to predominate and expose these cells to phagocytic clearance through PrCR. Although we did not find changes in the numbers of MZMs, they likely contributed to the clearance of MZ B cells in our experiments. Early clinical trial

results indicate that targeting the CD47/SIRPα axis is highly beneficial in B cell malignancies, especially in combination with therapeutic Abs against CD19 or CD20 (38). It is possible that part of this success is attributable to CD47 being one of only a few critical don't eat me signals expressed by healthy and malignant B cells. It will be beneficial for further studies to examine the specific monocyte or macrophage populations responsible for clearance.

We also found that blockade of CD47 led to an increase in myeloid-recruiting chemokines. We propose that CD47 levels and CCL2 production are inversely linked, and this is one way through which CD47 blockade actively mobilizes and recruits Ly6C^{hi} monocytes. We also observed, as would be expected, that the inflammatory monocytes infiltrating the blood and the macrophages migrating to the spleen highly expressed SIRPα and the β_2 integrin CD11b/MAC1. CD11b^{+} cells were also seen to cluster in the splenic red pulp, cuffing arterioles upon CD47 blockade, reminiscent of the CCL2-dependent macrophage clustering reported for MZMs (data not shown) (39). Furthermore, SIRPα has specifically been shown to be involved in integrin-mediated, CCL2-dependent migration (40). It is unclear why blockade of CD47 would lead to increased CCL2 production, and future studies should examine the connection between these molecules. The connection between SIRPα and β_2 integrins in CCL2 responsiveness presents an interesting avenue of future investigation, as β_2 integrins have also recently been shown to be a critical component of CD47 blockade-induced PrCR (41). As CD47, originally named integrin-associated protein, interacts with both SIRPα and integrins, it will be important to investigate which of these interactions is impacting CCL2 production.

Acknowledgments

We thank members of the Weissman and Hasenkrug laboratories for helpful advice and discussions and A. Lee, A. McCarty, T. Naik, and L. Quinn for administrative and logistical support. We thank Yael Rosenberg-Hasson and the staff of the Stanford Human Immune Monitoring Center for expertise and for running the mouse Luminex assays, and the Stanford Institute for Stem Cell Biology and Regenerative Medicine FACS Core for providing technical support.

Disclosures

I.L.W. was a cofounder, director, and stockholder in Forty Seven Inc., a public company that was involved in CD47-based immunotherapy of cancer during this study but was subsequently acquired by Gilead. At the time of this submission, I.L.W. has no formal relationship with Gilead. The other authors have no financial conflicts of interest.

References

1. Oldenborg, P. A., A. Zheleznyak, Y. F. Fang, C. F. Lagenaur, H. D. Gresham, and F. P. Lindberg. 2000. Role of CD47 as a marker of self on red blood cells. *Science* 288: 2051–2054.
2. Jaiswal, S., M. P. Chao, R. Majeti, and I. L. Weissman. 2010. Macrophages as mediators of tumor immunosurveillance. *Trends Immunol.* 31: 212–219.
3. Barclay, A. N., and T. K. Van den Berg. 2014. The interaction between signal regulatory protein alpha (SIRPα) and CD47: structure, function, and therapeutic target. *Annu. Rev. Immunol.* 32: 25–50.
4. Lagasse, E., and I. L. Weissman. 1994. bcl-2 inhibits apoptosis of neutrophils but not their engulfment by macrophages. *J. Exp. Med.* 179: 1047–1052.
5. Chao, M. P., R. Majeti, and I. L. Weissman. 2011. Programmed cell removal: a new obstacle in the road to developing cancer. *Nat. Rev. Cancer* 12: 58–67.
6. Bian, Z., L. Shi, Y. L. Guo, Z. Lv, C. Tang, S. Niu, A. Tremblay, M. Venkataramani, C. Culpepper, L. Li, et al. 2016. Cd47-Sirpα interaction and IL-10 constrain inflammation-induced macrophage phagocytosis of healthy self-cells. *Proc. Natl. Acad. Sci. USA* 113: E5434–E5443.
7. Burger, P., P. Hilarius-Stokman, D. de Korte, T. K. van den Berg, and R. van Bruggen. 2012. CD47 functions as a molecular switch for erythrocyte phagocytosis. *Blood* 119: 5512–5521.
8. Willingham, S. B., J.-P. Volkmer, A. J. Gentles, D. Sahoo, P. Dalerba, S. S. Mitra, J. Wang, H. Contreras-Trujillo, R. Martin, J. D. Cohen, et al. 2012. The CD47-signal regulatory protein alpha (SIRPa) interaction is a therapeutic target for human solid tumors. *Proc. Natl. Acad. Sci. USA* 109: 6662–6667.
9. Jaiswal, S., C. H. M. Jamieson, W. W. Pang, C. Y. Park, M. P. Chao, R. Majeti, D. Traver, N. van Rooijen, and I. L. Weissman. 2009. CD47 is upregulated on circulating hematopoietic stem cells and leukemia cells to avoid phagocytosis. *Cell* 138: 271–285.
10. Legrand, N., N. D. Huntington, M. Nagasawa, A. Q. Bakker, R. Schotte, H. Strick-Marchand, S. J. de Geus, S. M. Pouw, M. Böhne, A. Voordouw, et al. 2011. Functional CD47/signal regulatory protein alpha (SIRPα) interaction is required for optimal human T- and natural killer- (NK) cell homeostasis in vivo. *Proc. Natl. Acad. Sci. USA* 108: 13224–13229.
11. Chhabra, A., A. M. Ring, K. Weiskopf, P. J. Schnorr, S. Gordon, A. C. Le, H. S. Kwon, N. G. Ring, J. Volkmer, P. Y. Ho, et al. 2016. Hematopoietic stem cell transplantation in immunocompetent hosts without radiation or chemotherapy. *Sci. Transl. Med.* 8: 351ra105.
12. Majeti, R., M. W. Becker, Q. Tian, T. L. M. Lee, X. Yan, R. Liu, J. H. Chiang, L. Hood, M. F. Clarke, and I. L. Weissman. 2009. Dysregulated gene expression networks in human acute myelogenous leukemia stem cells. *Proc. Natl. Acad. Sci. USA* 106: 3396–3401.
13. Chao, M. P., A. A. Alizadeh, C. Tang, M. Jan, R. Weissman-Tsukamoto, F. Zhao, C. Y. Park, I. L. Weissman, and R. Majeti. 2011. Therapeutic antibody targeting of CD47 eliminates human acute lymphoblastic leukemia. *Cancer Res.* 71: 1374–1384.
14. Majeti, R., M. P. Chao, A. A. Alizadeh, W. W. Pang, S. Jaiswal, K. D. Gibbs, Jr., N. van Rooijen, and I. L. Weissman. 2009. CD47 is an adverse prognostic factor and therapeutic antibody target on human acute myeloid leukemia stem cells. *Cell* 138: 286–299.
15. Chao, M. P., A. A. Alizadeh, C. Tang, J. H. Myklebust, B. Varghese, S. Gill, M. Jan, A. C. Cha, C. K. Chan, B. T. Tan, et al. 2010. Anti-CD47 antibody synergizes with rituximab to promote phagocytosis and eradicate non-Hodgkin lymphoma. *Cell* 142: 699–713.
16. Zhao, X. W., E. M. van Beek, K. Schornagel, H. Van der Maaden, M. Van Houdt, M. A. Otten, P. Finetti, M. Van Egmond, T. Matozaki, G. Kraal, et al. 2011. CD47-signal regulatory protein-α (SIRPα) interactions form a barrier for antibody-mediated tumor cell destruction. *Proc. Natl. Acad. Sci. USA* 108: 18342–18347.
17. Zhang, M., G. Hutter, S. A. Kahn, T. D. Azad, S. Gholamin, C. Y. Xu, J. Liu, A. S. Achrol, C. Richard, P. Sommerkamp, et al. 2016. Anti-CD47 treatment stimulates phagocytosis of glioblastoma by M1 and M2 polarized macrophages and promotes M1 polarized macrophages in vivo. *PLoS One* 11: e0153550.
18. Krampitz, G. W., B. M. George, S. B. Willingham, J.-P. Volkmer, K. Weiskopf, N. Jahchan, A. M. Newman, D. Sahoo, A. J. Zemek, R. L. Yanovsky, et al. 2016. Identification of tumorigenic cells and therapeutic targets in pancreatic neuroendocrine tumors. [Published erratum appears in 2016 *Proc. Natl. Acad. Sci. USA* 113: E5538.] *Proc. Natl. Acad. Sci. USA* 113: 4464–4469.
19. Edris, B., K. Weiskopf, A. K. Volkmer, J. P. Volkmer, S. B. Willingham, H. Contreras-Trujillo, J. Liu, R. Majeti, R. B. West, J. A. Fletcher, et al. 2012. Antibody therapy targeting the CD47 protein is effective in a model of aggressive metastatic leiomyosarcoma. *Proc. Natl. Acad. Sci. USA* 109: 6656–6661.
20. Gallagher, S., S. Turman, K. Lekstrom, S. Wilson, R. Herbst, and Y. Wang. 2017. CD47 limits antibody dependent phagocytosis against non-malignant B cells. *Mol. Immunol.* 85: 57–65.
21. Karlsson, M. C. I., R. Guinamard, S. Bolland, M. Sankala, R. M. Steinman, and J. V. Ravetch. 2003. Macrophages control the retention and trafficking of B lymphocytes in the splenic marginal zone. *J. Exp. Med.* 198: 333–340.
22. Snapper, C. M., H. Yamaguchi, M. A. Moorman, R. Sneed, D. Smoot, and J. J. Mond. 1993. Natural killer cells induce activated murine B cells to secrete Ig. *J. Immunol.* 151: 5251–5260.
23. Oliver, A. M., F. Martin, G. L. Gartland, R. H. Carter, and J. F. Kearney. 1997. Marginal zone B cells exhibit unique activation, proliferative and immunoglobulin secretory responses. *Eur. J. Immunol.* 27: 2366–2374.
24. Weiskopf, K., N. S. Jahchan, P. J. Schnorr, S. Cristea, A. M. Ring, R. L. Maute, A. K. Volkmer, J. P. Volkmer, J. Liu, J. S. Lim, et al. 2016. CD47-blocking immunotherapies stimulate macrophage-mediated destruction of small-cell lung cancer. *J. Clin. Invest.* 126: 2610–2620.
25. Shi, C., and E. G. Pamer. 2011. Monocyte recruitment during infection and inflammation. *Nat. Rev. Immunol.* 11: 762–774.
26. Jones, D. D., J. R. Wilmore, and D. Allman. 2015. Cellular dynamics of memory B cell populations: IgM^{+} and IgG^{+} memory B cells persist indefinitely as quiescent cells. *J. Immunol.* 195: 4753–4759.
27. Kolan, S. S., A. Boman, T. Matozaki, K. Lejon, and P. A. Oldenborg. 2015. Lack of non-hematopoietic SIRPα signaling disturbs the splenic marginal zone architecture resulting in accumulation and displacement of marginal zone B cells. *Biochem. Biophys. Res. Commun.* 460: 645–650.
28. Li, L.-X., S. M. Atif, S. E. Schmiel, S.-J. Lee, and S. J. McSorley. 2012. Increased susceptibility to *Salmonella* infection in signal regulatory protein α-deficient mice. *J. Immunol.* 189: 2537–2544.
29. Shultz, L. D., D. R. Coman, C. L. Bailey, W. G. Beamer, and C. L. Sidman. 1984. "Viable motheaten," a new allele at the motheaten locus. I. Pathology. *Am. J. Pathol.* 116: 179–192.
30. Harder, K. W., L. M. Parsons, J. Armes, N. Evans, N. Kountouri, R. Clark, C. Quilici, D. Grail, G. S. Hodgson, A. R. Dunn, and M. L. Hibbs. 2001. Gain- and loss-of-function Lyn mutant mice define a critical inhibitory role for Lyn in the myeloid lineage. *Immunity* 15: 603–615.

31. Harder, K. W., C. Quilici, E. Naik, M. Inglese, N. Kountouri, A. Turner, K. Zlatic, D. M. Tarlinton, and M. L. Hibbs. 2004. Perturbed myelo/erythropoiesis in Lyn-deficient mice is similar to that in mice lacking the inhibitory phosphatases SHP-1 and SHIP-1. *Blood* 104: 3901–3910.
32. Xiao, W., H. Hong, Y. Kawakami, C. A. Lowell, and T. Kawakami. 2008. Regulation of myeloproliferation and M2 macrophage programming in mice by Lyn/Hck, SHIP, and Stat5. *J. Clin. Invest.* 118: 924–934.
33. Feng, M., J. Y. Chen, R. Weissman-Tsukamoto, J. P. Volkmer, P. Y. Ho, K. M. McKenna, S. Cheshier, M. Zhang, N. Guo, P. Gip, et al. 2015. Macrophages eat cancer cells using their own calreticulin as a guide: roles of TLR and Btk. *Proc. Natl. Acad. Sci. USA* 112: 2145–2150.
34. Byrne, J. C., J. Ní Gabhann, K. B. Stacey, B. M. Coffey, E. McCarthy, W. Thomas, and C. A. Jefferies. 2013. Bruton's tyrosine kinase is required for apoptotic cell uptake via regulating the phosphorylation and localization of calreticulin. *J. Immunol.* 190: 5207–5215.
35. Martin, F., and J. F. Kearney. 2002. Marginal-zone B cells. *Nat. Rev. Immunol.* 2: 323–335.
36. Qian, Y., H. Wang, and S. H. Clarke. 2004. Impaired clearance of apoptotic cells induces the activation of autoreactive anti-Sm marginal zone and B-1 B cells. *J. Immunol.* 172: 625–635.
37. Dillon, S. R., A. Constantinescu, and M. S. Schlissel. 2001. Annexin V binds to positively selected B cells. *J. Immunol.* 166: 58–71.
38. Advani, R., I. Flinn, L. Popplewell, A. Forero, N. L. Bartlett, N. Ghosh, J. Kline, M. Roschewski, A. LaCasce, G. P. Collins, et al. 2018. CD47 blockade by Hu5F9-G4 and rituximab in non-Hodgkin's lymphoma. *N. Engl. J. Med.* 379: 1711–1721.
39. Jablonska, J., K. E. Dittmar, T. Kleinke, J. Buer, and S. Weiss. 2007. Essential role of CCL2 in clustering of splenic ERTR-9^{+} macrophages during infection of BALB/c mice by *Listeria monocytogenes*. *Infect. Immun.* 75: 462–470.
40. Alenghat, F. J., Q. J. Baca, N. T. Rubin, L. I. Pao, T. Matozaki, C. A. Lowell, D. E. Golan, B. G. Neel, and K. D. Swanson. 2012. Macrophages require Skap2 and Sirpα for integrin-stimulated cytoskeletal rearrangement. *J. Cell Sci.* 125: 5535–5545.
41. Chen, J., M. C. Zhong, H. Guo, D. Davidson, S. Mishel, Y. Lu, I. Rhee, L. A. Pérez-Quintero, S. Zhang, M. E. Cruz-Munoz, et al. 2017. SLAMF7 is critical for phagocytosis of haematopoietic tumour cells via Mac-1 integrin. *Nature* 544: 493–497.